Altenau, E. H., Pavelsky, T. M., Moller, D., Pitcher, L. H., Bates, P. D., Durand, M. T., & Smith, L. C. (2019). Temporal variations in river water surface elevation and slope captured by AirSWOT. *Remote Sensing of Environment*, *224*, 304-316. https://doi.org/10.1016/j.rse.2019.02.002

Temporal Variations in River Water Surface Elevation and Slope Captured by AirSWOT

Elizabeth H. Altenau[1], Tamlin M. Pavelsky[1], Delwyn Moller[2], Lincoln H Pitcher[3], Paul D. Bates[4], Michael T. Durand[5], and Laurence C. Smith[3]

[1]Department of Geological Sciences, University of North Carolina, Chapel Hill, USA

[2]Remote Sensing Solutions, Inc., Pasadena, CA, USA

[3]Department of Geography, University of California, Los Angeles, USA

[4]School of Geographical Sciences, University of Bristol, UK

[5]School of Earth Science, and Byrd Polar and Climate Research Center, The Ohio State University, Columbus, USA

Corresponding Author: Elizabeth Humphries Altenau (ealtenau@unc.edu)

Abstract

The Surface Water and Ocean Topography (SWOT) satellite mission aims to improve the frequency and accuracy of global observations of river water surface elevations (WSEs) and slopes. As part of the SWOT mission, an airborne analog, AirSWOT, provides spatially-distributed measurements of WSEs for river reaches tens to hundreds of kilometers in length. For the first time, we demonstrate the ability of AirSWOT to consistently measure temporal dynamics in river WSE and slope. We evaluate data from six AirSWOT flights conducted between June 7-22, 2015 along a ~90 km reach of the Tanana River, AK. To validate AirSWOT measurements, we compare AirSWOT WSEs and slopes against an in situ network of 12 pressure transducers (PTs). Assuming error-free in situ data, AirSWOT measurements of river WSEs have an overall root mean square difference (RMSD) of 11.8 cm when averaged over 1 km^2 areas whilst measurements of river surface slope have an RMSD of 1.6 cm/km for reach lengths >5 km. AirSWOT is also capable of recording accurate river WSE changes between flight dates, with an RMSD of 9.8 cm. Regrettably, observed in situ slope changes that transpired between the six flights are well below AirSWOT's accuracy, limiting the evaluation of AirSWOT's ability to capture temporal changes in slope. In addition to validating the direct AirSWOT measurements, we compare discharge values calculated via Manning's equation using AirSWOT WSEs and slopes to discharge values calculated using PT WSEs and slopes. We define or calibrate the remaining discharge parameters using a combination of in situ and remotely sensed observations, and we hold these remaining parameters constant between the two types of calculations to evaluate the impact of using AirSWOT versus the PT observations of WSE and slope. Results indicate that AirSWOT-derived discharge estimates are similar to the PT-derived discharge estimates, with an RMSD of 13.8%. Additionally, 42% of the AirSWOT-

based discharge estimates fall within the PT discharge estimates' uncertainty bounds. We conclude that AirSWOT can measure multitemporal variations in river WSE and spatial variations in slope with both high accuracy and spatial sampling, providing a compelling alternative to in situ measurements of regional-scale, spatiotemporal fluvial dynamics.

1. Introduction

The recent and rapid expansion of remote sensing technologies provides exciting opportunities to address global-scale questions of fluvial process, especially in areas where in situ observations are limited (Hannah et al., 2011; Pavelsky et al., 2014). Currently, the most robust method for space-based observation of river water surface elevation (WSE) and slope is satellite altimetry (Bates et al., 2014; Calmant et al., 2008; Tourian et al., 2016). A number of studies use available altimeters to measure WSEs with accuracies ranging from 10 cm (ICESat, SARAL/Altika) to several decimeters (TOPEX/Poseidon, Jason-2, Envisat) (Calmant et al., 2008; O'Loughlin et al., 2016). These altimeter measurements have been used to validate flood models, create time series of water level changes, estimate discharge, and quantify river height and slope variability in inaccessible river basins (Domeneghetti, 2016; Garambois et al., 2016; Kouraev et al., 2004; Papa et al., 2010; Paris et al., 2016; Tourian et al., 2016). However, altimeter missions and their processing chains were primarily developed to measure sea surface dynamics. As a result, altimeter observations of surface water bodies have complex error characteristics due to variable waveforms, river or lake WSE changes within the altimeter footprint, surrounding land elevations, and specular reflections (Alsdorf et al., 2007; Calmant et al., 2008). Additionally, altimeters have low temporal (10-35 days) and spatial (70-600 m) resolutions, along with large spatial gaps between orbital paths, which is not ideal for viewing surface water dynamics. These characteristics limit the hydraulic visibility, the potential to

capture hydrological responses and hydraulic variabilities within a river network using remote sensing, of the world's largest river systems to altimetry (Alsdorf et al., 2007; Calmant et al., 2008; Garambois et al., 2016; Maillard et al., 2015; Smith, 1997).

The upcoming Surface Water and Ocean Topography (SWOT) mission plans to vastly increase global observations of rivers 100 m wide and larger by providing 3-D measurements of river WSEs from ~78°N to ~78°S (Biancamaria et al., 2016; Fjørtoft et al., 2014). SWOT's goal is to measure river WSEs with an accuracy of 10 cm or better when averaged over 1 km^2 areas and river surface slopes with an accuracy of 1.7 cm/km or better along 10 km reaches (Rodriguez, 2016). As part of the SWOT mission, NASA has developed AirSWOT, an airborne Ka-band interferometer that produces data products analogous to SWOT (Altenau et al., 2017b; Biancamaria et al., 2016; Fu et al., 2015). AirSWOT is designed to measure high-accuracy WSEs in a ~5 km wide swath that enables mapping of river reaches hundreds of kilometers in length within a reasonable timeframe. Whilst there are some differences between AirSWOT's incidence angles and planned SWOT viewing geometry, AirSWOT provides comparable measurements to SWOT by recording elevations at the same radar wavelength (Ka-Band) and at narrower incidence angles (~4-25°) than existing sensors. More detailed summaries of the differences between AirSWOT and SWOT, along with AirSWOT's capabilities, are presented by Moller et al. (2011) and Altenau et al. (2017b).

Previous work has shown that for a single day, AirSWOT can capture detailed spatial variations in river WSEs and slopes with accuracies of 8-9 cm over 1 km^2 areas and 1-1.5 cm/km over 10 km reaches. These results suggest that AirSWOT is capable of obtaining SWOT-like measurements within the mission error requirements and is useful for understanding river hydraulics at scales that will be unobservable by SWOT (Altenau et al., 2017b, Pitcher et al.,

2018). To date, however, AirSWOT has been tested against data from a single flight. The ability of AirSWOT to accurately measure temporal variations in river WSEs and slopes remains unknown. AirSWOT continues to be an experimental instrument with processing algorithms under development. Furthermore, varying aircraft stability and roughness of the water surface affect radar returns and impact AirSWOT's accuracy. Therefore, it is imperative to validate AirSWOT measurements across and between collection days, in addition to the previously published single-day results.

For the first time, we demonstrate the ability of AirSWOT to record river WSE and slope changes between six different AirSWOT collections acquired over a three-week period. Furthermore, we investigate the value of using AirSWOT measurements to estimate other hydraulic quantities by comparing discharge calculated using AirSWOT WSEs and slopes versus in situ WSEs and slopes, combined with other in situ and remotely sensed observations of depth and width, in Manning's Equation.

2. Study Site

For this study, we conducted a six-week field campaign from May 15, 2015 to June 27, 2015 along a ~90 km reach of the Tanana River, Alaska, USA (Fig. 1a). This site is ideal for assessment of AirSWOT's capabilities to measure WSEs and slopes over a highly-dynamic, multichannel river offering challenges for AirSWOT beyond those of single-threaded, low relief rivers. The shape of the annual hydrograph on the Tanana is dominated by melt of snowpack and glaciers during the spring and summer. Mean annual discharge for the open-water season (May to October) at the Nenana gauge station from 1962 to 2015 is ~1299 m^3/s. The mean daily discharge for the duration of the field campaign was 870 m^3/s, which is very low for that time of year. For comparison, the mean daily discharge for June 2016 was 1113 m^3/s. There are three

primary tributaries that flow into the main study reach: Salchaket Slough, Chena River, and Wood River. Based on the U.S. Geological stream gauges 15485500 Tanana River at Fairbanks, AK and 15515500 Tanana River at Nenana, AK, these tributaries likely account for about ~20% of the flow between the two gauge stations on average. The glacial origin of the Tanana River results in a high sediment load, which interacts with local topography to produce a complex morphology that ranges from highly braided to a single meandering channel (Brabets et al., 2000). This varied river morphology, in combination with ubiquitous sandbars and high bluffs (20-50 m high), makes the Tanana a challenging test site for AirSWOT's InSAR technology (Altenau et al., 2017b).

3. Methods

3.1 Field Measurements

To validate AirSWOT measurements of river WSE and slope, we installed a network of 20 Solinst M5 Levelogger Edge pressure transducers (PTs) throughout the study reach to record high-resolution, in situ measurements of changes in river height as well as two Solinst Barologgers to compensate for atmospheric pressure fluctuations (https://www.solinst.com/products/data/3001.pdf). Eight of the 20 pressure transducers are not used in this study because they were buried by mobile sediment or riverbanks after installation as a result of fluvial geomorphological processes. This left us with 12 viable pressure transducers to calculate river height and slope changes (Fig. 1a). To deploy the PTs, we secured each device to a cinderblock that was attached to the end of a long metal cable tethered to a fixed-point on the bank of the river, usually a tree. We then placed the cinder block into the river about 5-10 m from the bank. The distance between PTs ranged from 0.29-23 km, with the majority of the PTs spaced 4-8 km apart. Data were recorded at 2 min intervals. Reported accuracy for the PTs is

±0.3 cm and ±0.05 kPa (0.5 cm) for the Barologgers, resulting in a combined instrument accuracy for water level measurements of ±0.8 cm (https://www.solinst.com/products/data/3001.pdf).

To convert the water depth measurements from the PTs to river WSEs, we used an optical survey level to measure the height difference between the water surface and GPS benchmarks (metal rods) that we placed near the fixed-point on the bank at each PT location. We used the Canadian Spatial Reference System Precise Point Positioning tool (CSRS-PPP) provided by Natural Resources Canada for static post-processing of the GPS surveys, providing centimeter-level accuracies of the absolute WSEs collected at each PT site (http://www.nrcan.gc.ca/earth-sciences/geomatics/geodetic-reference-systems/). The accuracy of the GPS surveys ranges from ±3.6-6.3 cm, while our optical survey accuracy is ±0.2 cm, bringing the total uncertainty for the PTs to ±4.6-7.3 cm. It is also possible that the PTs experienced some shifting or sinking due to the high mobility of the Tanana River bed (Brabets et al., 2000). Any potential movements would add to the uncertainty in the PT WSEs. However, we did not have robust methods for measuring these effects, therefore they are not accounted for in our uncertainty calculations. A solid earth tide correction is accounted for in the AirSWOT processing methodology, but not in the GPS post-processing. As a result, we apply a solid earth tide correction to the PT WSE values using the program *solid* (http://geodesyworld.github.io/SOFTS/solid.htm#link0).

In addition to the PTs, we collected a high-resolution GPS profile along the main channel of the study reach on June 7, 2015 (Fig. 1a). We collected the profile using a Trimble R9 survey-grade GPS system attached to the back of an 8.5 m river boat. GPS profile measurements were post-processed using the CSRS-PPP tool in kinematic processing mode and provide nearly

continuous observations of river heights with ~3 m spacing between points and an uncertainty of ±2.0 cm in the vertical (Altenau et al., 2017b). Along with the river WSEs, we collected water depths at each GPS profile point using a single-beam SonarMite Echo Sounder v.3.0. Instrument accuracy for the echo sounder is ±2.5 cm (http://www.ohmex.com/sonarmite.html).

3.2 AirSWOT Measurements

After installation of the PTs, six AirSWOT datasets were collected on June 7, June 9, June 16, June 17, June 18, and June 22, 2015, to image temporal fluctuations in river WSE and slope. Each AirSWOT mission consists of 4-24 overlapping flight lines per day, resulting in a total of 66 individual lines of AirSWOT WSE measurements. The June 9th and June 16th collections contain 24 flight lines covering a 43 km reach along the upstream portion of the field site and a 32 km reach along the downstream portion of the field site, while the remaining flight days each contain 4-6 flight lines of data covering the entire 90 km study reach (Fig. 1b-g).

The AirSWOT team at NASA's Jet Propulsion Laboratory processes the AirSWOT data using custom software. Each AirSWOT flight line consists of 4 products, with the primary product being the AirSWOT elevations measured in meters above the WGS84 ellipsoid. Other products provided with the elevations are the relative radar backscatter (dB), incidence angle (°) and estimated elevation errors (m). Estimated elevation errors are calculated from the phase variance (Cramer-Rao bound) which is based on the correlation between the two interferometric images and depends on the sensor incidence angles, radar wavelength, and underlying surface type (high topography, vegetation type, soil moisture, etc.) (Altenau et al., 2017b; Rosen et al., 2000). All AirSWOT products are in a raster format and have a pixel resolution of 3.6 m in a UTM 6N projection.

3.3 2-D AirSWOT Filtering

In this paper, we focus on the ability of AirSWOT to record changes in river WSEs and slopes. To do so, we filter the 2-D AirSWOT measurements before spatially averaging and comparing them to the PT surveys. Filtering the 2-D signal removes pixels containing WSE outliers that are often due to layover and improper estimation of the ambiguity height parameter. The ambiguity height is the amount of height change that leads to a 2π change in the interferometric phase and is a key parameter in unwrapping the interferometric phase to calculate elevation values (Rosen et al., 2000). When using near-nadir geometry, layover tends to occur in environments with moderate-to-high topography, and the ambiguity heights have a faster range variation (Neeck et al., 2012). As a result, calculating ambiguity heights can be more difficult, especially in the near-swath and in areas adjacent to higher topography. Incorrect ambiguity heights often lead to high vertical errors and geolocation errors in WSEs (Biancamaria et al., 2016).

The first step in the filtering process is isolating the river pixels in the AirSWOT data. For each AirSWOT line, we use a binary river mask created from a three-band color infrared (CIR) camera (http://cirrus-designs.com/) on board the AirSWOT platform to isolate the river pixels from surrounding land pixels. Regrettably, the majority of CIR images collected during the AirSWOT flights were cloudy, which prevents us from using automatic methods to create an independent river mask for each date. The CIR imagery were clear for the June 17th flight, however, so we use these data to create a river mask and filter out the land pixels in each AirSWOT line. We produce the river mask using a normalized difference water index (NDWI) transformation with a threshold of 0.3 to identify water pixels (McFeeters, 1996). All pixels greater than the threshold are assigned a value of one for water, and any pixels less than the threshold are assigned a value of zero. Due to the high turbidity of the Tanana River, some

uncertainty in the water mask is introduced based on the chosen water threshold. As a result, water pixels with high suspended sediment concentrations could be classified as land, or conversely, land pixels that have NDWI values close to the chosen water threshold could be classified as water. These misclassified pixels in the water mask could increase the noise in the identified AirSWOT WSE pixels. Additionally, the river on June 17th was at a lower stage than the majority of the data collections with the exception of June 16th, which had a stage about 5 cm lower than June 17th. Therefore, the river extent observed in the river mask should be comparable to June 16th, but is likely to exclude some inundated pixels on the other collection days.

Once the river WSEs are isolated, we use a 2 km^2 moving window to remove extreme outliers by erasing pixels ±3 standard deviations away from the mean river WSE in the window (Altenau et al., 2017b). This filter helps eliminate pixels affected by layover from adjacent high topography and vegetation, as well as misclassified water/land pixels from the water mask. Despite the initial outlier filter, there are some large areas affected by ambiguity height errors that are not removed during the filtering process because they significantly affect the statistics within the 2 km^2 window. Therefore, we manually remove the incorrect pixels in these areas (Fig. 2). These larger areas of ambiguity height errors are prominent in 9 of the 66 AirSWOT lines. Fig. 3a shows the effects of the 2-D filtering process on the distribution of WSEs for all the AirSWOT flights. Overall, ~95% of the pixels are retained during the initial 2-D filtering.

3.4 WSE Validation

After filtering the 2-D AirSWOT measurements, we spatially average the WSEs and slopes before comparing AirSWOT to the PT observations. Spatial averaging is commonly applied to interferometric measurements in order to reduce random errors that are independent from pixel to pixel (Rodriguez and Martin, 1992). The SWOT mission accuracy requirement for

river WSEs of 10 cm is based on averaging pixels within 1 km^2 areas, a threshold the SWOT Science Team has determined will allow significant scientific advances in fluvial hydrology (Rodriguez, 2016). Therefore, we use this area requirement as a baseline for assessing AirSWOT's capabilities for capturing same-day river WSEs as well as their changes over time (Altenau et al., 2017b). To quantify WSE differences between AirSWOT and the in situ measurements for each flight date, we calculate a weighted average of the filtered AirSWOT WSEs within 1 km^2 areas around each PT using the following equation:

$$\bar{x} = \frac{\sum_{i=1}^{n} x_i w_i}{\sum_{i=1}^{n} w_i} \quad (1)$$

where $\bar{x}$ is the weighted average of the AirSWOT WSEs at a single PT location, x_i is the AirSWOT WSE for each pixel (i), and w_i is the weight associated with each pixel and is determined by AirSWOT's estimated elevation error (e_i, see Section 3.2):

$$w_i = \frac{1}{{e_i}^2} \quad (2)$$

As a result, pixels with lower estimated errors have more influence in the final weighted average than the pixels with larger estimated errors.

Despite the initial 2-D filtering of the AirSWOT WSEs, some remaining erroneous pixels affected by ambiguity height errors are still present in the data. These pixels tend to have large vertical offsets compared to field observations but low e_i values, resulting in comparatively high errors in the weighted average calculation. To reduce the effects of these pixels, we calculate the median for each 1 km^2 area and retain 70% of the AirSWOT WSEs that surround the median value. We also eliminate pixels that have estimated errors of < 0.1 m because we find these particularly low error estimates often correspond with pixels that are affected by ambiguity

252 height errors. Pixels with estimated errors < 0.1 m make up less than 1% of the data, therefore
253 this second filter preserves about 70% of the data within each 1 km^2 area while reducing the
254 errors in the weighted average that are caused by the incorrect pixels. The spatial filtering within
255 the 1 km^2 areas and application of the weighted mean reduces the mean average difference
256 (MAD) between AirSWOT and PT WSEs by 68% compared to calculating a simple mean on the
257 unfiltered data (Fig. 3b).

258 It is difficult to calculate uncertainties for the averaged WSEs using the AirSWOT data
259 alone. We can calculate the random error component of the uncertainty for the averaged
260 AirSWOT WSEs based on the weights (w_i):

$$uncertainty = \frac{\sqrt{F}}{\sqrt{\sum_{i=1}^{n} w_i}} \tag{3}$$

261 where *F* is a factor that accounts for the oversampling of pixels within the gridded UTM product
262 relative to the sampling assumed when estimating the elevation errors. *F* depends on the
263 incidence angle (*I*):

$$F = \frac{0.52}{\sin(I)} \tag{4}$$

264 The constant 0.52 comes from the ratio (1.87 m)/(3.6 m) where 1.87 m is the effective spatial
265 resolution for 80 MHz bandwidth and 3.6 m is the UTM posting. Equation 3 accounts for the
266 random error component (noise on the interferometric phase) in the AirSWOT measurement
267 uncertainty, but does not include systematic errors that are due to variations in antenna pointing
268 and incomplete knowledge of the airborne platform location such as attitude errors, baseline
269 errors, and position errors (Rodriguez and Martin, 1992; Rosen et al., 2000). As a result, the
270 uncertainties calculated using equation 3, which range from 0.1 – 2.0 cm, only account for a

small fraction of the total error and are unrealistically low. Systematic errors in the AirSWOT data affect the accuracy of the WSEs, and likely add to the random error uncertainty, but cannot be quantified from the data itself or from available ancillary information. Rather than present misleading uncertainty values, we elect to not designate uncertainties for the averaged AirSWOT WSEs, and focus instead on reporting observed differences between the AirSWOT and PT measurements, as this comparison provides an empirical estimate of the total error.

Once the averaged AirSWOT WSEs are determined, we calculate the same-day, absolute differences and associated root-mean-square differences (RMSDs) between the AirSWOT and PT WSEs. Although Altenau et al. (2017b) report no bias in the June 9th AirSWOT measurements along the Tanana River, we observe a spatially consistent negative bias across the AirSWOT WSEs that ranges from -8 cm to -20 cm depending on the collection day. The AirSWOT data presented in this paper are processed using different methods from the data presented in Altenau et al. (2017b), and we have not determined the source of the bias in the current data at this time. Possible explanations for the bias include improper common range calibrations, differences in how solid earth tide corrections are incorporated, erroneous GPS solutions, and problems with the troposphere correction. As a result, we subtract the mean bias on each day from the AirSWOT WSEs and recalculate the absolute differences and RMSDs between the same-day, bias-corrected AirSWOT measurements and PT WSEs (Table 1).

In addition to the same-day WSEs, we calculate WSE change values for the PTs and bias-corrected AirSWOT measurements between the first AirSWOT date (June 7th) and all subsequent dates (n = 58), as well as WSE changes between all possible AirSWOT date combinations (n = 161). We estimate uncertainties for the PT WSE changes by taking the root sum of squares of the uncertainties in the daily PT WSEs. Finally, we calculate the absolute

differences and RMSDs between the bias-corrected AirSWOT and PT WSE change observations.

3.5 Slope Validation

Using different combinations of the 12 PT locations, we identify a total of 63 pairs of PT sites (e.g. PT01 and PT05) for calculating along-flow river surface slopes with reach lengths between PT points ranging from 5.1 to 83.6 km. At reach lengths <5 km AirSWOT slopes become severely affected by high-variability noise likely resulting from layover and ambiguity height errors. Therefore, PT combinations with reach lengths <5 km are not included here. For each PT pair, we calculate the PT surface slopes by dividing the difference in WSE by the reach length between the PT sites.

To compare the PT slopes to AirSWOT slopes, we first create 1-D, high-resolution AirSWOT profiles by extracting the 2-D AirSWOT WSE measurements coincident to the GPS profile locations collected in the field (Fig. 1a). At each GPS profile point, we calculate a 1 km orthogonal vector across the Tanana River and use equation 3.1 to calculate a weighted mean of the 2-D AirSWOT WSEs along the orthogonal vector. After the weighted averaging, we create the final 1-D AirSWOT profiles by applying a running median filter with a window of 500 pixels (~1600 m) to eliminate large peaks in the initial profiles (Fig. 4). The running median filter reduces high frequency variability, which is unrealistic for a large river like the Tanana. We validate the running median filter by comparing the initial profile and filtered profile on June 7th to the GPS profile WSEs that were also collected on June 7th. When compared to the GPS profile, applying the running median filter reduces the final AirSWOT profile RMSD to 18.6 cm versus 69.3 cm for the initial AirSWOT profile (Fig. 5). While a window size of 500 pixels works well for the Tanana River profile, optimal window size will likely vary among river

317 environments depending on topography, morphology, size, and other factors. Currently,
318 knowledge about the field site, or in situ observations, are required to determine the optimal
319 window size for smoothing. However, future measurements from the SWOT satellite mission
320 will provide river WSE profiles with higher accuracies than existing digital elevation models
321 (Langhorst et al., unpublished results), which will aid in applying this methodology to ungauged
322 or hard to access rivers.

323 Once the 1-D WSE profiles are created, we use ordinary least squares linear regressions
324 to calculate same-day slopes along the AirSWOT profiles between each of the 63 PT pair
325 locations. We estimate AirSWOT slope uncertainties using the linear regressions, and the PT
326 slope uncertainties by calculating the difference between the maximum and minimum slopes for
327 each PT pair, which are based on the PT WSE uncertainties. To validate AirSWOT slope
328 measurements, we calculate absolute differences and RMSDs between the same-day AirSWOT
329 and PT slopes (Table 1). Due to equipment constraints, we do not have high-resolution GPS
330 profiles along the study reach for each separate AirSWOT flight and are limited to validating
331 temporal fluctuations in AirSWOT slopes against the PT observations. Therefore, we use linear
332 regressions to calculate AirSWOT slopes over more sophisticated methods, such as LOESS
333 filters, because we cannot validate spatial variations in AirSWOT slopes against the PT
334 measurements. Altenau et al. (2017b) present results regarding AirSWOT's ability to capture
335 detailed spatial variations in WSE and slope along the same study reach of the Tanana River.

336 Next, we calculate the slope changes between the first AirSWOT date (June 7th) and all
337 subsequent dates (n = 297), as well as all possible AirSWOT date combinations (n = 766). To
338 estimate uncertainties for the slope changes, we take the root sum of squares of the uncertainties
339 in the same-day PT and AirSWOT slopes. We then calculate absolute differences for the

AirSWOT and PT slope changes between June 7th and all subsequent dates, and slope changes between all possible date combinations.

3.6 Discharge Estimation

In addition to validating AirSWOT's ability to capture temporal fluctuations in river WSE and slope, we assess how AirSWOT observations compare to PT observations of WSE and slope when calculating discharge at each PT location using Manning's equation (Manning et al., 1890):

$$Q = \frac{1}{n} A R^{2/3} \sqrt{S} \tag{5}$$

where Q is the discharge, A is the cross sectional area, R is the hydraulic radius, S is the river surface slope, and n is Manning's roughness coefficient.

First, we estimate the cross sectional area at each PT location. To derive depths, we use the bathymetric measurements collected with the echo sounder (see Section 3.1) to identify the average river bed elevation, or lowest point in a cross section, at each PT location. The bed elevation measurements were collected independently of the PT measurements and stay constant in time at each PT site. We derive the temporally-varying depth values used to calculate the cross sectional area at each PT site by subtracting the static bed elevations from the temporally varying PT and AirSWOT WSEs (Altenau et al., 2017a).

For cross sectional widths, we use the CIR imagery collected during each AirSWOT flight to manually measure the river widths at the various PT sites on each day, since the clouds in the imagery inhibit us from using automatic width detection methods. Two PTs lack width measurements for several days due to dense cloud cover (PT07) and fewer AirSWOT observations (PT10). Therefore, we exclude these PTs in the discharge estimation, leaving us ten PT locations to calculate discharge. To test the effect of channel geometry on the calculated

362 discharge values, we perform a sensitivity analysis for 4 different cross sectional shapes
363 (rectangle, parabola, triangle, and trapezoid). For the trapezoidal cross section, we assume the
364 base width is half the top width. We find a negligible (0.2%) effect on mean discharge
365 differences between cross sectional shapes, therefore, we use a simple rectangular geometry to
366 calculate cross sectional area by multiplying the river width by depth.
367 Next, we estimate the river surface slope at each cross section by locating the closest
368 upstream and downstream PTs to the current PT location and calculating the slope between the
369 two bounding sites. The two exceptions are the first and last PT locations #1 (PT01) and #12
370 (PT12) for which we use the closest downstream and upstream location only to calculate the
371 slopes. For example, we determine the slope for PT05 by calculating the slope between PT04
372 and PT06, and we determine PT01's slope by calculating the slope between PT01 and PT02.
373 Finally, we calibrate temporally-varying roughness coefficients at each PT site by
374 calculating PT discharge estimates over a range of roughness values (0.01-0.1) and comparing
375 the estimates to in situ discharge values from the Nenana gauge station at the downstream end of
376 the study reach (Fig. 1a, Table 2). We assess how well AirSWOT measurements compare to the
377 PT measurements of WSE and slope when estimating discharge by calculating daily and overall
378 RMSD values between the PT and AirSWOT discharge values. The goal in this analysis is to
379 compare discharge values calculated using AirSWOT measurements of WSE and slope to
380 discharge values calculated using the PT measurements of WSE and slope, holding all other
381 variables constant, not to invert discharge values using mass conserved flow law inversion
382 methods like those discussed by Durand et al. (2016). Because we calibrate Manning's n to the
383 gauge station discharge, the discharge values we calculate are not independent of the gauge, and
384 we do not attempt to compare the discharge estimates to the gauge observations or analyze the

effects of tributary inputs at the different PT locations. We do, however, display the Nenana gauge discharge values for reference.

4. Results

Spatial patterns and biases in the differences between the same-day AirSWOT and PT WSEs are similar across all days, which indicates the separate AirSWOT flights are affected by comparable error sources (Fig. 6a,c; Table 1). RMSDs for the same-day, bias-corrected AirSWOT WSEs range from 8.3 cm to 15.0 cm with an overall RMSD of 11.8 cm. The consistency in the same-day AirSWOT WSE differences and biases allows AirSWOT to capture the same general pattern in temporal WSE changes as the PTs, with an RMSD of 9.8 cm for all possible date combinations (Fig. 7). Had the same-day WSE differences shown variable patterns and bias directions for each AirSWOT flight, high-accuracy WSE changes would be less detectable. Between the different PT locations, AirSWOT WSE change differences shift from underestimations upstream to overestimations downstream (Fig. 7c). The variations in WSE change differences between the PT sites are likely due to the different environmental conditions at each location and how they affect the radar returns. High topography, water surface roughness, width and number of channels in a cross section, and bare versus vegetated banks all influence the strength and quality of the radar returns at a specific PT location. For example, PT10 displays a comparatively large range in WSE change differences (Fig. 7c). PT10 is directly adjacent to an area of high topography, making it susceptible to layover errors, and is not covered by the high observational density June 9th and June 16th AirSWOT collections, leaving only data collections with fewer observations in the calculation of WSE changes.

In addition to the WSEs, AirSWOT is able to measure river surface slopes with an RMSD of 1.6 cm/km, and 98% of slope differences fall below 3.0 cm/km for reach lengths ≥5

km (Table 1, Fig. 6d). Same-day slope differences increase as reach length decreases. Unfortunately, the Tanana River slopes do not significantly change between the six AirSWOT collection days, though slight increases in slope, within the margin of error, are observed by the PTs as stage decreases (Fig. 8a). Mean slope changes observed by the PTs from June 7th to all subsequent dates ranged from 0.07 cm/km to 0.17 cm/km. These observed slope changes are well below AirSWOT's slope accuracy, but variations in mean AirSWOT slope change are similarly low, ranging from -0.35 cm/km to 0.26 cm/km (Fig. 8a). Additionally, AirSWOT displays lower slope uncertainties than the PTs due to the high spatial density of the AirSWOT measurements with slope uncertainties decreasing exponentially as reach length increases (Fig. 8b).

Both PT and AirSWOT discharge estimates capture the general hydrograph pattern observed by the Nenana gauge station, with discharge decreasing until June 16th and increasing thereafter (Fig. 9). AirSWOT discharge values display a 13.8% difference compared to the PT values, on average, with RMSDs ranging from 11.1% to 18.0% (Table 3). 42% of the AirSWOT discharge estimates fall within the PT discharge uncertainty bounds. Discharge differences are predominately related to the AirSWOT WSE differences. A linear regression between discharge differences and WSE differences (R^2=0.88) shows a 1.1% increase in discharge difference with every centimeter of WSE difference (Fig. 10a). Conversely, there is no statistically significant relationship between AirSWOT slope differences and discharge differences, with an R^2=0.03 (Fig. 10b).

5. Discussion and Conclusion

In this study, we present a first analysis of AirSWOT's ability to observe temporal variations in river WSE and slope over variable reach lengths and timescales. Altenau et al.

(2017b) and Pitcher et al. (2018) document AirSWOT's ability to record accurate river WSEs and slopes for one collection date, while here we analyze the consistency of AirSWOT measurements over the course of three weeks and six different flights. It is not always straightforward for AirSWOT to measure same-day river WSEs due to errors and biases likely related to the movement of the aircraft, variations in water surface roughness, and difficulties in phase unwrapping at narrower incidence angles (<5°) (Biancamaria et al., 2016, Neeck et al., 2012). Comparisons with PT observations illustrate that AirSWOT accurately captures temporal water surface fluctuations along a complex, anabranching river system, with an RMSD of 11.8 cm for same-day WSEs (Fig, 6c., Table 2). Given the differences between the PT and AirSWOT same-day WSEs display consistent patterns between flight collections, AirSWOT is also able to capture decimeter-level WSE changes, with an RMSD of 9.8 cm for all possible date combinations (Fig. 7c). Some of the differences between the AirSWOT and the PT WSEs could be due to the spatial averaging of the AirSWOT data or the PT uncertainty (±4.6-7.3 cm), which is a result of the instrument and GPS survey errors. PTs provide WSE measurements at a specific location in the cross section. Due to superelevation, the PTs could record different WSE values depending on whether they were placed on the inside or outside of a meander bend. These cross-sectional effects on WSE would be observable by PTs if they were placed appropriately in the channel, but they are below the accuracy of the 2-D AirSWOT signal. Averaging over 1 km^2 areas, which is required to achieve decimeter-level accuracies in the AirSWOT WSEs, also results in averaging out any superelevation signal.

In contrast to river WSEs, AirSWOT is capable of producing robust river surface slope measurements with an RMSD of 1.6 cm/km for same-day slopes for reach lengths ≥5 km (Table 2). While the slope changes observed along the Tanana River are significantly smaller than

AirSWOT's daily slope accuracy, it is important to note that AirSWOT does detect extremely low temporal variability in slopes similar to the PT measurements (Fig. 8a). This low slope variability over time is somewhat surprising considering the dip in the hydrograph that occurs during the measurement period (Fig. 1a). We suggest several possible explanations for the low temporal variability in slopes along the Tanana River: (1) The rate of discharge change is actually quite low (±30 m^3/s/day) compared to the rates of change associated with snowmelt and rainfall hydrographs moving through this reach of the Tanana. As a result, the 'wave' generated by this discharge change has relatively low amplitude and varies more gradually than is typical for this system. (2) Surface water slopes along this river reach may have strong 'base level control' by width constrictions due to the adjacent high bluffs and geologic setting. (3) There is some evidence that temporal variability in water slope is low for other anabranching river systems. For example, O'Loughlin et al. (2013) found only ~0.15 cm/km of slope change between the falling and rising limbs of the hydrograph along the middle reach of the Congo River. Additional research is needed during more extreme hydrologic events, or along rivers with larger slope variability over time, in order to draw definitive conclusions regarding AirSWOT's accuracy in observing temporal slope changes.

In addition to validating AirSWOT's direct measurements of river WSE and slope, we test the effectiveness of the AirSWOT observations for approximating discharge compared to the PT observations. To do so, we use Manning's equation to calculate and compare discharge values using both the PT and AirSWOT measurements of river WSE and slope. We hold the other discharge parameters constant between the PT and AirSWOT calculations, and derive them from additional in situ (depth, Manning's n) and remotely sensed observations (width). Discharge estimates calculated using AirSWOT measurements of WSE and slope result in

marginal differences compared to discharge estimates calculated using the PT observations of WSE and slope. On average, AirSWOT discharge estimates are within 13.8% of the estimates attained using the PTs, and 42% of the time AirSWOT discharge measurements fall within the PT discharge uncertainty (Table 3). For the Tanana River, AirSWOT WSE differences dominate the observed discharge differences, with slope differences showing little effect (Fig. 10). This result is likely due, in part, to the limited slope variations occurring throughout the Tanana River during the field campaign. Because development of AirSWOT processing methods is ongoing, AirSWOT WSE errors and biases are likely to decrease in the future, along with a corresponding decrease in discharge errors. When combined with sophisticated algorithms and appropriate parameters, AirSWOT measurements can be used to invert discharge fluctuations along inaccessible and unmonitored river networks (Bjerklie et al., 2005; Bonnema et al., 2016; Durand et al., 2016; Hagemann et al., 2017), potentially including rivers that are too small to observe using satellite sensors yet have important biogeochemical and ecological impacts (Allen and Pavelsky, 2018; King et al., 2018).

Despite the challenges inherent in making precise measurements of WSEs when using an airborne radar, AirSWOT provides a compelling alternative to current remote sensing and in situ observations for measuring river dynamics. AirSWOT's slope measurements are particularly notable due to their high accuracy and spatial density. In situ river gauging stations, or pressure transducers, provide accurate WSE measurements at one location, but are not ideal for estimating slope variability along river reaches due to their coarse spatial coverage. For example, gauge stations are typically spaced tens to hundreds of kilometers apart and have limited placement options due to equipment functionality and accessibility constraints (Allen and Pavelsky, 2015; Bates, 2004; Hannah et al., 2011). In addition to in situ methods, studies using nadir altimeter

data to estimate river slopes contend with poor spatial resolutions, wide track spacings between observations, and significant height uncertainties (Garambois et al., 2016; O'Loughlin et al., 2013, 2016). In contrast, AirSWOT can provide spatially distributed measurements of WSE along hundreds of kilometers of river, which can capture detailed spatial variabilities in river WSEs and provide better-constrained slope estimates compared to in situ sensors and satellite altimeters (Altenau et al., 2017b).

In addition to spaceborne observations, alternative airborne sensors insufficiently measure river WSEs and slopes. Specifically, airborne LiDAR systems, which are known for their high-accuracy measurements of land surfaces, tend to provide poorer returns over open water surfaces due to the absorption of the laser beam within the water column, low signal-to-noise ratios, and high occurrences of specular reflection (Antonarakis et al., 2008; Sanders, 2007; Schumann et al., 2008; Smith et al., 2009). As a result, most studies that utilize LiDAR measurements over inland waters focus on classifying water body areas not WSE or slope (Antonarakis et al., 2008; Crasto et al., 2015; Höfle, 2009). Recently, Branch et al. (2018) and Hudson et al. (2017) used airborne LiDAR transects to map river WSEs and slopes along the Columbia River Estuary. They found spatially-averaged LiDAR WSEs agreed with a local tide gauge to within an RMSE of ~40 cm, but had difficulty deriving precise slope estimates from the LiDAR data due to under sampling and sampling error. These results suggest AirSWOT provides superior measurements of river WSEs and slope compared to alternative LiDAR systems.

Though AirSWOT data is not available globally, it presents an opportunity to study regional hydraulics and hydrology in novel ways (Altenau et al., 2017b; Pitcher et al., 2018). Current and future projects combine AirSWOT observations with other spaceborne and airborne sensors including LiDAR, multispectral, and hyperspectral imagers to study interactions between

surface water dynamics, geochemical fluxes, and geomorphic processes. The Arctic-Boreal Vulnerability Experiment (AboVE) (https://above.nasa.gov/about.html), ongoing, combines in situ observations including WSE, methane, and CO_2 with remotely sensed data products of WSE (AirSWOT), soil moisture, and water quality to better understand the fast changing ecosystem dynamics in arctic and boreal regions. Additionally, the recently funded Delta-X project plans to combine in situ data, model outputs, and remote sensing observations from a variety of airborne sensors, including AirSWOT, to improve current understanding of water partitioning and sedimentation dynamics in the Mississippi River Delta. Furthermore, measurements of river WSEs and slopes from AirSWOT can be used for calibration, validation, and assimilation into local and regional-scale flood models to improve their performance by providing similar, and often superior, accuracies and better spatiotemporal coverage than existing airborne and satellite sensors. Finally, results from this study and others indicate AirSWOT accuracies consistently meet the SWOT mission accuracy requirements for river processes (Altenau et al., 2017b, Pitcher et al., 2018), which suggests AirSWOT could be a valuable tool for validating future SWOT measurements of river WSE and slope in complex and hard to reach river basins with little in situ data.

A**cknowledgements**

This work was funded by NASA Terrestrial Hydrology Program Grant # NNX13AD05G, managed by Jared Entin. Field locations and observations of water surface elevation were based on equipment services provided by the UNAVCO Facility with support from the National Science Foundation (NSF) and National Aeronautics and Space Administration (NASA) under NSF Cooperative Agreement No. EAR-0735156. Laurence C. Smith acknowledges additional support from NASA #NNX16AH85G and Paul D. Bates is supported by a Leverhulme Research

Fellowship and a Royal Society Wolfson Research Merit award. We acknowledge Curtis Chen, Craig Stringham, Albert Chen, Xiaaoqing Wu, Gregory Sadowy, and the JPL AFRC AirSWOT teams for collection and processing of the AirSWOT data, as well as John Arvesen from Cirrus Digital Systems for processing the CIR imagery. We also want to thank our boat driver Sam Demientieff for his navigational expertise on the Tanana River, which allowed for safe and timely data collection. Finally, we would like to thank the three anonymous reviewers who provided comments that helped improve the quality of the manuscript. All of the data in the main text are presented in the figures and may be obtained from Elizabeth H. Altenau (email: ealtenau@unc.edu).

REFERENCES

Allen, G.H., Pavelsky, T., 2018. Global extent of rivers and streams. Science (80-.). 361, 585–588. https://doi.org/10.1126/science.aat063

Allen, G.H., Pavelsky, T.M., 2015. Patterns of river width and surface area newly revealed by the satellite-derived North American River Width (NARWidth) dataset. Geophys. Res. Lett. 1–14. https://doi.org/10.1002/2014GL062764.Received

Alsdorf, D.E., Rodríguez, E., Lettenmaier, D.P., 2007. Measuring surface water from space. Rev. Geophys. 45, RG2002. https://doi.org/10.1029/2006RG000197

Altenau, E.H., Pavelsky, T.M., Bates, P.D., Neal, J.C., 2017a. The effects of spatial resolution and dimensionality on modeling regional-scale hydraulics in a multichannel river. Water Resour. Res. 53, 1683–1701. https://doi.org/10.1002/2016WR019396

Altenau, E.H., Pavelsky, T.M., Moller, D., Lion, C., Pitcher, L.H., Allen, G.H., Bates, P.D., Calmant, S., Durand, M., Smith, L.C., 2017b. AirSWOT measurements of river water surface elevation and slope: Tanana River, AK. Geophys. Res. Lett. 1–9. https://doi.org/10.1002/2016GL071577

Antonarakis, A.S., Richards, K.S., Brasington, J., 2008. Object-based land cover classification using airborne LiDAR. Remote Sens. Environ. 112, 2988–2998. https://doi.org/10.1016/j.rse.2008.02.004

Bates, P.D., 2004. Remote sensing and flood inundation modelling. Hydrol. Process. 18, 2593–2597. https://doi.org/10.1002/hyp.5649

Bates, P.D., Neal, J.C., Alsdorf, D., Schumann, G.J.-P., 2014. Observing Global Surface Water Flood Dynamics. Surv. Geophys. 35, 839–852. https://doi.org/10.1007/s10712-013-9269-4

Biancamaria, S., Lettenmaier, D.P., Pavelsky, T.M., 2016. The SWOT Mission and Its Capabilities for Land Hydrology. Surv. Geophys. 37, 307–337. https://doi.org/10.1007/s10712-015-9346-y

Bjerklie, D.M., Moller, D., Smith, L.C., Dingman, S.L., 2005. Estimating discharge in rivers using remotely sensed hydraulic information. J. Hydrol. 309, 191–209. https://doi.org/10.1016/j.jhydrol.2004.11.022

Bonnema, M.G., Sikder, S., Hossain, F., Durand, M., Gleason, C., Bjerklie, D.M., 2016. Benchmarking wide swath altimetry-based river discharge estimation algorithms for the Ganges river system. Water Resour. Res. 52, 5974–5997. https://doi.org/10.1002/2016WR018977.Received

Brabets, T.P., Wang, B., Meade, R.H., 2000. Environmental and Hydrologic Overview of the Yukon River Basin , Alaska and Canada. US Dep. Inter. US Geol. Surv.

Branch, R.A., Horner-Devine, A.R., Akan, C., Chickadel, C.C., Farquharson, G., Hudson, A., Talke, S.A., Thomson, J., Jessup, A.T., 2018. Airborne LiDAR Measurements and Model Simulations of Tides, Waves, and Surface Slope at the Mouth of the Columbia River. IEEE Trans. Geosci. Remote Sens. 56, 7038–7048. https://doi.org/10.1109/TGRS.2018.2847561

Calmant, S., Seyler, F., Cretaux, J.F., 2008. Monitoring continental surface waters by satellite altimetry. Surv. Geophys. 29, 247–269. https://doi.org/10.1007/s10712-008-9051-1

Crasto, N., Hopkinson, C., Forbes, D.L., Lesack, L., Marsh, P., Spooner, I., van der Sanden, J.J., 2015. A LiDAR-based decision-tree classification of open water surfaces in an Arctic delta. Remote Sens. Environ. 164, 90–102. https://doi.org/10.1016/j.rse.2015.04.011

Domeneghetti, A., 2016. On the use of SRTM and altimetry data for flood modeling in data-sparse regions. Water Resour. Res. 1–20. https://doi.org/10.1002/2014WR015716

Durand, M., Gleason, C., Garambois, P.A., Bjerklie, D., Smith, L.C., Roux, H., Rodríguez, E., Bates, P.D., Pavelsky, T.M., Monnier, J., Chen, X., Di Baldassarre, G., Fiset, J.-M., Flipo, N., Frasson, R.P. de M., Fulton, J., Goutal, N., Hossain, F., Humphries, E., Minear, J.T., Mukolwe, M.M., Neal, J.C., Ricci, S., Sanders, B.F., Schumann, G., Schubert, J.E., Vilmin, L., 2016. An intercomparison of remote sensing river discharge estimation algorithms frommeasurements of river height, width, and slope M. 613–615. https://doi.org/10.1029/2008WR006912.M

Fjørtoft, R., Gaudin, J.M., Pourthié, N., Lalaurie, J.C., Mallet, A., Nouvel, J.F., Martinot-Lagarde, J., Oriot, H., Borderies, P., Ruiz, C., Daniel, S., 2014. KaRIn on SWOT: Characteristics of near-nadir Ka-band interferometric SAR imagery. IEEE Trans. Geosci. Remote Sens. 52, 2172–2185. https://doi.org/10.1109/TGRS.2013.2258402

Fu, L.-L., Alsdorf, D., Morrow, R., Rodriguez, E., 2015. SWOT: The Surface Water and Ocean Topography Mission. SWOT NASA/JPL Proj. https://doi.org/10.1017/CBO9781107415324.004

Garambois, P., Calmant, S., Roux, H., Paris, A., Finaud-guyot, P., Montazem, A., Santos, J., Spatiales, O., Cnes, U.M.R., Ird, C., 2016. Hydraulic visibility : using satellite altimetry to parameterize a hydraulic model of an ungauged reach of a braided river. Hydrol. Process. 1–20. https://doi.org/10.1002/hyp.11033

Hagemann, M.W., Gleason, C.J., Durand, M.T., 2017. BAM: Bayesian AMHG-Manning Inference of Discharge Using Remotely Sensed Stream Width, Slope, and Height. Water Resour. Res. 53, 9692–9707. https://doi.org/10.1002/2017WR021626

Hannah, D.M., Demuth, S., van Lanen, H.A.J., Looser, U., Prudhomme, C., Rees, G., Stahl, K., Tallaksen, L.M., 2011. Large-scale river flow archives: Importance, current status and future needs. Hydrol. Process. 25, 1191–1200. https://doi.org/10.1002/hyp.7794

Höfle, B., 2009. "Water Surface Mapping from Airborne Laser Scanning using Signal Intensity and Elevation Data." Earth Surface Processes and Landforms 34 (12): 1635-1649. doi:10.1002/esp.1853.

Hudson, A.S., Talke, S.A., Branch, R., Chickadel, C., Farquharson, G., Jessup, A., 2017. Remote measurements of tides and river slope using an airborne lidar instrument. J. Atmos. Ocean. Technol. 34, 897–904. https://doi.org/10.1175/JTECH-D-16-0197.1

King, T. V., Neilson, B.T., Rasmussen, M.T., 2018. Estimating Discharge in Low-Order Rivers with High-Resolution Aerial Imagery. Water Resour. Res. 1–16. https://doi.org/10.1002/2017WR021868

Kouraev, A. V., Zakharova, E.A., Samain, O., Mognard, N.M., Cazenave, A., 2004. Ob' river discharge from TOPEX/Poseidon satellite altimetry (1992-2002). Remote Sens. Environ. 93, 238–245. https://doi.org/10.1016/j.rse.2004.07.007

Langhorst, T., T.M. Pavelsky, R.P.M. Frasson, R. Wei, A. Domeneghetti, E.H. Altenau, M.T. Durand, J.T. Minear, K. Wegmann, and M. Fuller, In Review. Anticipated improvements to in-river DEMs from the Surface Water and Ocean Topography mission, Frontiers in Earth Science.

Maillard, P., Bercher, N., Calmant, S., 2015. New processing approaches on the retrieval of water levels in Envisat and SARAL radar altimetry over rivers: A case study of the São Francisco River, Brazil. Remote Sens. Environ. 156, 226–241. https://doi.org/10.1016/j.rse.2014.09.027

Manning, R., Griffith, J. P., Pigot, T. F., & Vernon-Harcourt, L. F.,1890. On the flow of water in open channels and pipes. Transactions of the Institution of Civil Engineers of Ireland.

McFeeters, S.K., 1996. The use of the Normalized Difference Water Index (NDWI) in the delineation of open water features. Int. J. Remote Sens. 17, 1425–1432. https://doi.org/10.1080/01431169608948714

Moller, D., Rodríguez, E., Carswell, J., Esteban-Fernadez, D., 2011. A calibration/validation platform for the SWOT mission, in: Proc. International Geoscience and Remote Sensing Symposium. Vancouver, Canada.

Neeck, S.P., Lindstrom, E.J., Vaze, P. V., Fu, L.-L., 2012. Surface Water and Ocean Topography (SWOT) mission. Proc. SPIE 8533, Sensors, Syst. Next-Generation Satell. XVI 8533G. https://doi.org/10.1117/12.981151

O'Loughlin, F., Trigg, M.A., Schumann, G.J.P., Bates, P.D., 2013. Hydraulic characterization of the middle reach of the Congo River. Water Resour. Res. 49, 5059–5070. https://doi.org/10.1002/wrcr.20398

O'Loughlin, F.E., Neal, J., Yamazaki, D., Bates, P.D., 2016. ICESat-derived inland water surface spot heights. Water Resour. Res. 1–20. https://doi.org/10.1002/2014WR015716

Papa, F., Durand, F., Rossow, W.B., Rahman, A., Bala, S.K., 2010. Satellite altimeter-derived monthly discharge of the Ganga-Brahmaputra River and its seasonal to interannual variations from 1993 to 2008. J. Geophys. Res. Ocean. 115, 1–19. https://doi.org/10.1029/2009JC006075

Paris, A., Paiva, R.C.D., Silva, J.S., Moreira, D.M., Calmant, S., Garambois, P.-A., Collischonn, W., Bonnet, M.P., Seyler, F., 2016. Stage-discharge rating curves based on satellite altimetry and modeled discharge in the Amazon basin. Water Resour. Res. 1–20. https://doi.org/10.1002/2014WR015716

Pavelsky, T.M., Durand, M.T., Andreadis, K.M., Beighley, R.E., Paiva, R.C.D., Allen, G.H., Miller, Z.F., 2014. Assessing the potential global extent of SWOT river discharge observations. J. Hydrol. 519, 1516–1525. https://doi.org/10.1016/j.jhydrol.2014.08.044

Pitcher, L.H., Pavelsky, T.M., Smith, L.C., Moller, D.K., Altenau, E.H., Allen, G.H., Lion, C., Butman, D., Cooley, S.W., Fayne, J. and Bertram, M., 2018. AirSWOT InSAR mapping of surface water elevations and hydraulic gradients across the Yukon Flats Basin, Alaska. Water Resources Research.

Rodriguez, E., 2016. Surface Water and Ocean Topography Mission (SWOT) Project - Science Requirements Documents, SWOT NASA/JPL Project.

Rodriguez, E., Martin, J.M., 1992. Theory and design of interferometric synthetic aperture radars. IEE Proc. F Radar Signal Process. 139, 147. https://doi.org/10.1049/ip-f-2.1992.0018

Rosen, P.A., Hensley, S., Joughin, I.R., Li, F.K., Madsen, S.N., Rodriguez, E., Goldstein, R.M., 2000. Synthetic aperture radar interferometry Synthetic aperture radar interferometry. Proc. IEEE 88, 333–382. https://doi.org/10.1088/0266-5611/14/4/001

Sanders, B.F., 2007. Evaluation of on-line DEMs for flood inundation modeling. Adv. Water Resour. 30, 1831–1843. https://doi.org/10.1016/j.advwatres.2007.02.005

Schumann, G., Matgen, P., Cutler, M.E.J., Black, A., Hoffmann, L., Pfister, L., 2008. Comparison of remotely sensed water stages from LiDAR, topographic contours and SRTM. ISPRS J. Photogramm. Remote Sens. 63, 283–296. https://doi.org/10.1016/j.isprsjprs.2007.09.004

Smith, J.S., Chandler, J., Rose, J., 2009. High spatial resolution data acquisition for the geosciences: kite aerial photography. Earth Surf. Process. Landforms 34, 155–161. https://doi.org/10.1002/esp

Smith, L.C., 1997. SATELLITE REMOTE SENSING OF RIVER INUNDATION AREA , STAGE , AND DISCHARGE : A REVIEW. Hydrol. Process. 11, 1427–1439.
Tourian, M.J., Tarpanelli, A., Elmi, O., Qin, T., Brocca, L., Moramarco, T., Sneeuw, N., 2016. Spatiotemporal densification of river water level time series by multimission satellite altimetry. Water Resour. Res. 52, 1140–1159. https://doi.org/10.1002/2015WR017654

TABLES:

Table 1: Root-mean-square differences (RMSDs) and bias between the AirSWOT and pressure transducer same-day water surface elevations (WSEs) and along-flow slopes.

Date	WSE RMSD (cm)	Mean WSE Bias (cm)	WSE RMSD, Bias removed (cm)	Slope RMSD (cm/km)
June 7	18.2	-14.6	10.8	1.4
June 9	17.2	-8.1	15.0	1.8
June 16	24.2	-20.7	11.1	1.8
June 17	12.5	-9.3	8.3	1.6
June 18	19.3	-15.4	11.6	1.7
June 22	19.2	-13.3	12.7	1.2
All Days	18.8	-13.6	11.8	1.6

Table 2: Manning's equation parameters for each pressure transducer cross section.

Pressure Transducer	Width Range (m)	Number of Channels in Cross Section	Manning's n Range
1	468-654	5	0.065-0.095
2	413-458	4	0.055-0.080
3	321-326	1	0.045-0.055
4	468-616	6	0.055-0.085
5	462-619	6	0.045-0.080
6	354-458	4	0.045-0.070
8	267-305	2	0.035-0.055
9	209-258	2	0.025-0.035
11	297-382	2	0.035-0.065
12	259-279	1	0.035-0.045

Table 3: Root-mean-square differences (RMSDs) between AirSWOT and pressure transducer discharge estimates.

Date	RMSD (m^3/s)	RMSD (%)
June 7	105.8	11.1
June 9	148.1	18.0
June 16	107.9	15.6
June 17	85.4	11.9
June 18	98.6	12.6
June 22	117.9	12.6
All Days	112.3	13.8

FIGURES:

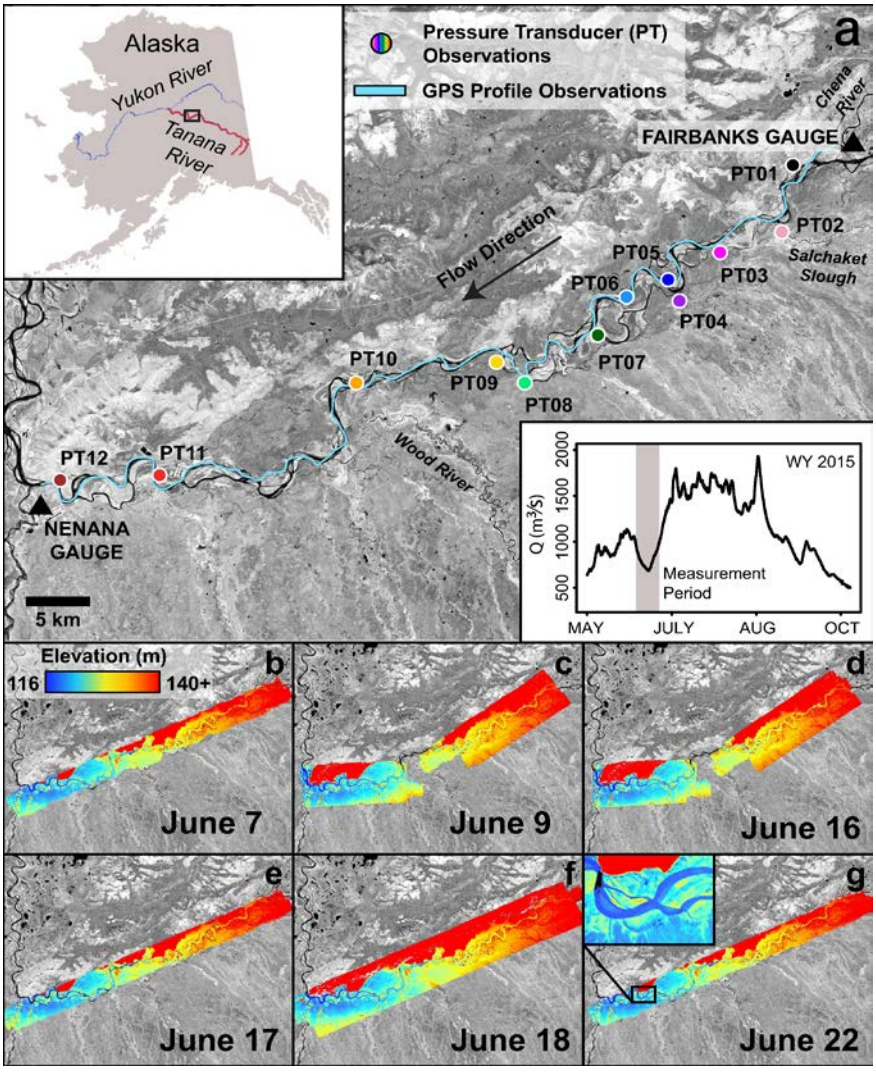

Fig. 1: a) Tanana River study reach depicted with a Landsat 8 near-infrared image acquired on June 15, 2015. Pressure transducer (PT) locations are indicated by the different colored circles and GPS profile measurements are indicated by the light blue line. Upper left inset displays the study reach location within the state of Alaska. Lower right inset displays the Nenana gauge hydrograph during the open water season for the 2015 water year (WY). The grey shaded area within the hydrograph shows the timeframe of the field campaign. b-g) AirSWOT extent and elevation mosaics for the six different flights.

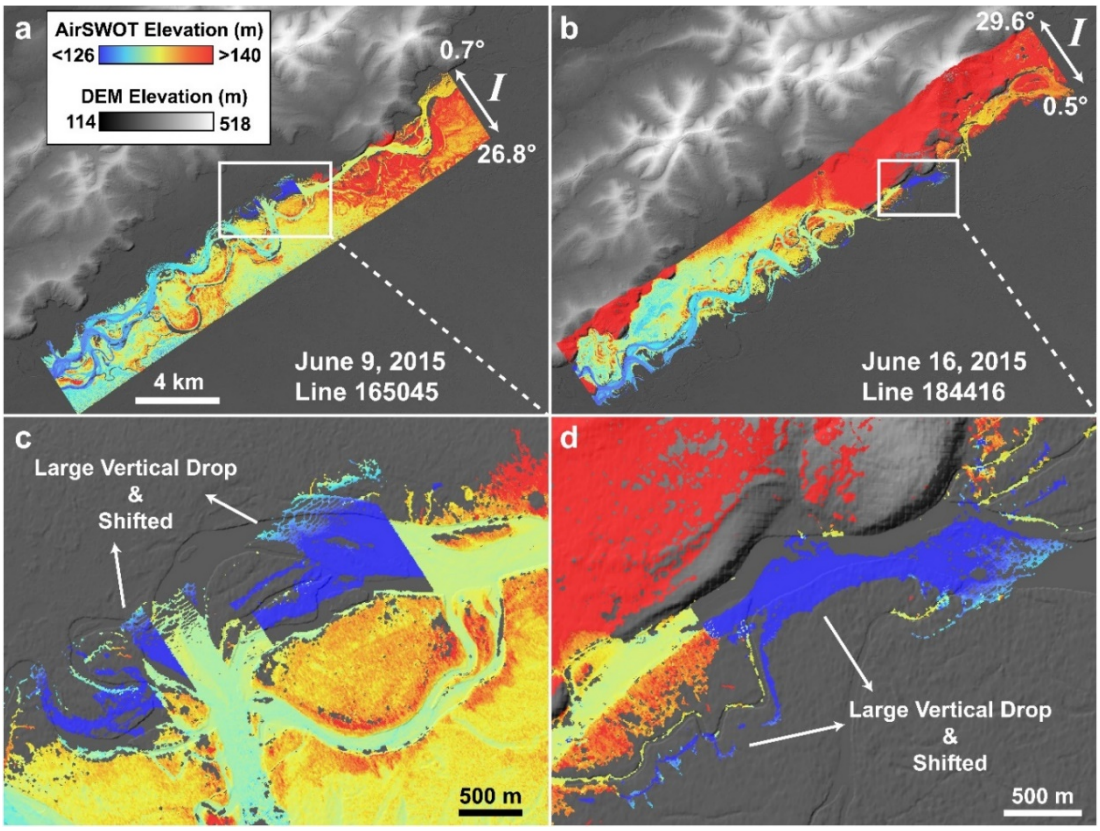

Fig. 2: Examples of ambiguity height errors in two AirSWOT lines from June 9, 2015 and June 16, 2015. The areas of dark blue pixels, which designate significant vertical drops and geolocation errors, are manually removed.

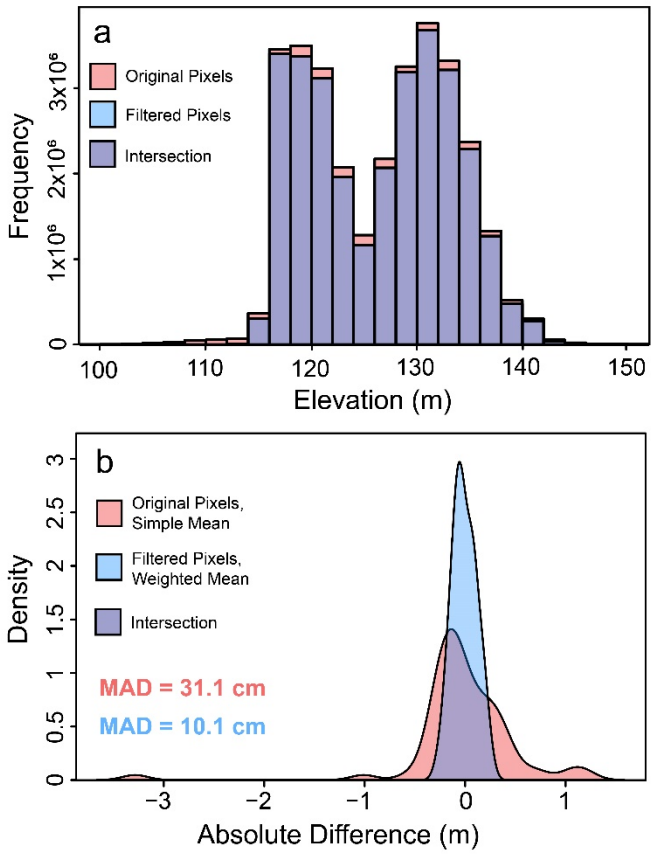

Fig 3: (a) Histograms of the AirSWOT WSE pixels from all six flight collections before (red) and after (blue) the 2-D spatial filtering. (b) Density plots of the absolute differences between the spatially-averaged AirSWOT and PT WSEs with (blue) and without (red) the 2-D filtering and weighted mean calculation. Mean absolute difference (MAD) values for each method are shown.

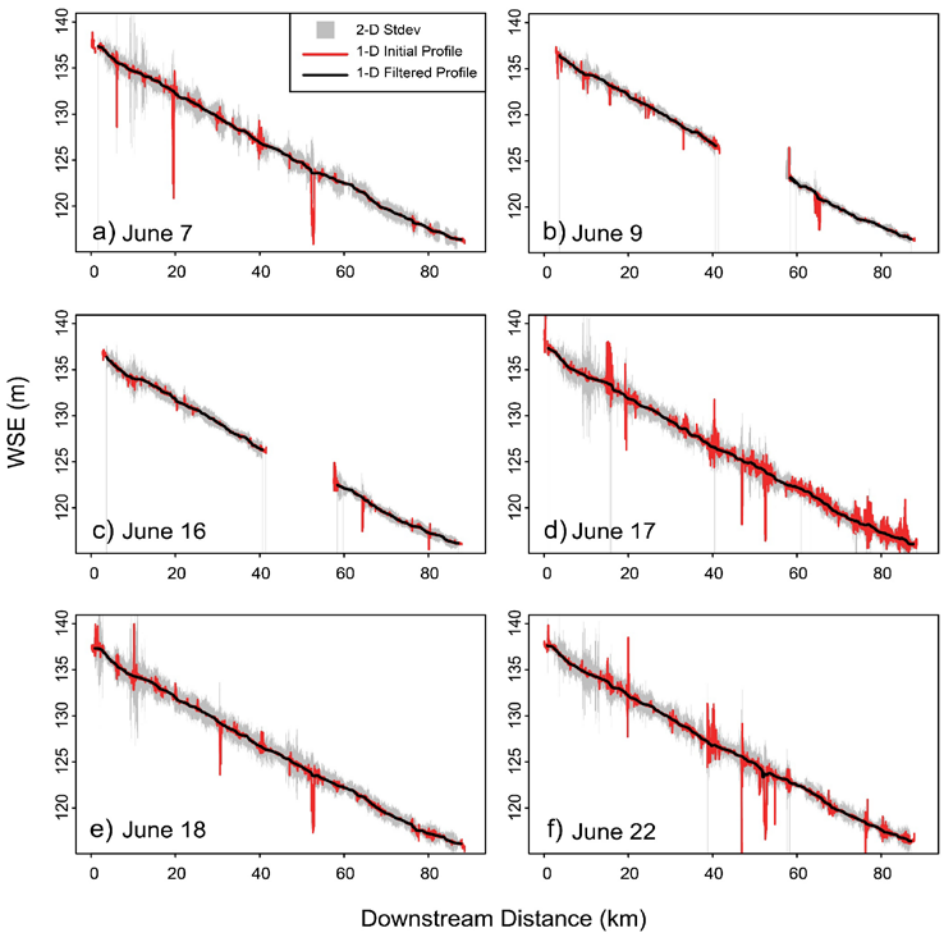

Fig. 4: AirSWOT river water surface elevation (WSE) profiles. The initial 1-D AirSWOT profiles (red) are produced by calculating a weighted mean of the 2-D AirSWOT pixels. Severe peaks in the initial 1-D profiles are removed using a running median filter with a window size of 500 observations (~1600 m) to yield the final profiles (black). The final profiles are used to calculate river surface slopes and slope changes. Standard deviations (Stdev) for the 2-D AirSWOT pixels measured across the orthogonal at each GPS profile observation are shown in grey.

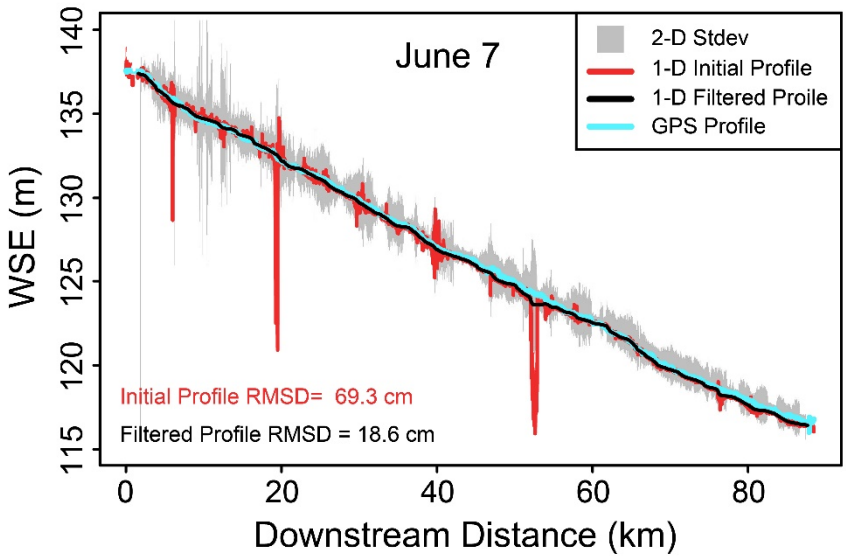

Fig. 5: AirSWOT water surface elevation (WSE) profile versus GPS profile on June 7, 2015. Standard deviations of the 2-D AirSWOT pixels across the orthogonal at each GPS profile observation are shown in grey. The final 1-D AirSWOT profiles (black) are created using a running-median filter with a window size of 500 observations (~1600 m) along the initial profiles (red). Root mean square differences (RMSD) between the two AirSWOT profiles and GPS profile (blue) are displayed.

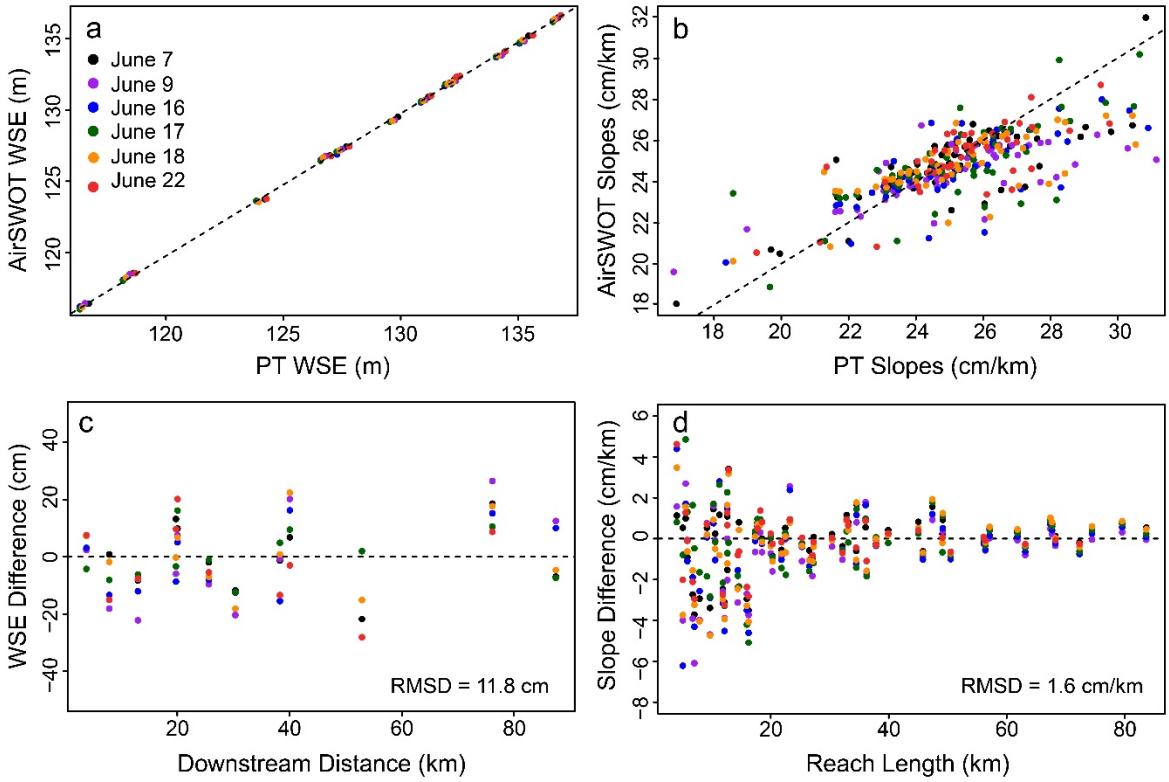

Fig. 6: AirSWOT vs. pressure transducer (PT) WSEs (a) and slopes (b). Dashed diagonal lines indicate the 1:1 lines. AirSWOT WSE (c) and slope (d) differences compared to the PTs for the various AirSWOT collections. AirSWOT WSEs and WSE differences are shown with the daily mean biases removed. Dashed horizontal lines indicate zero height and slope differences.

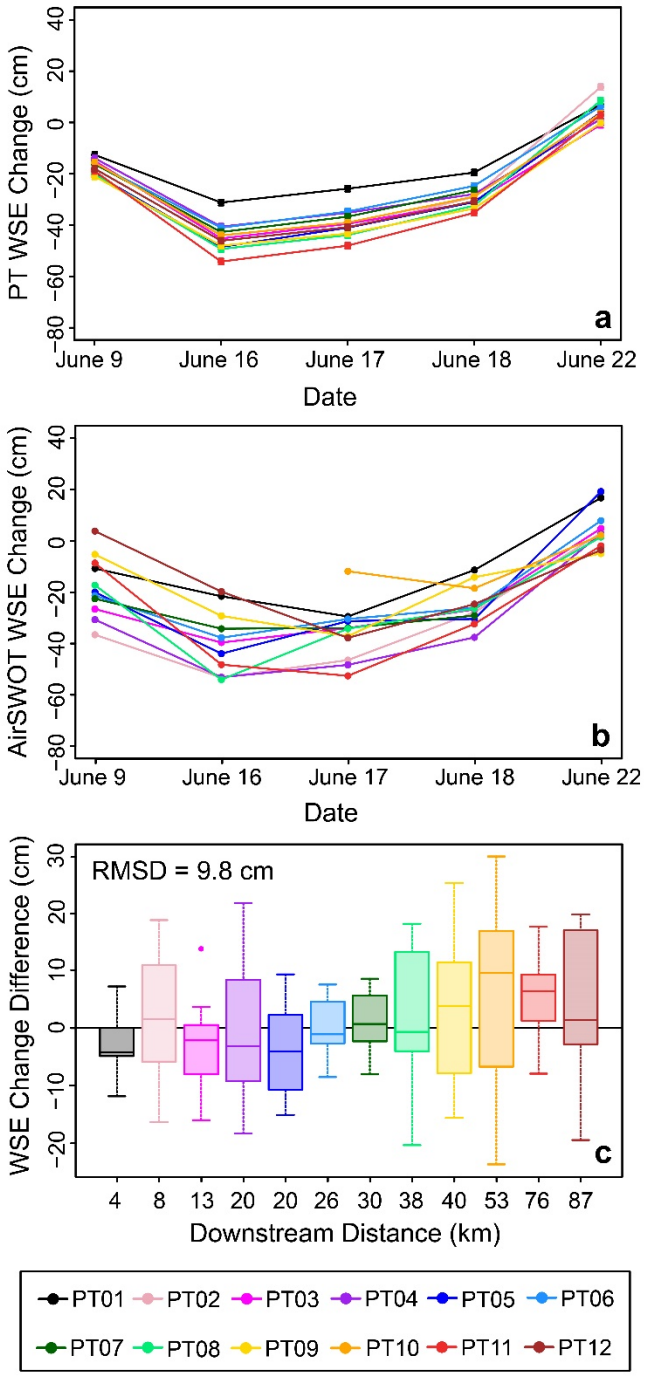

Fig. 7: Pressure transducer (PT) (a) and AirSWOT (b) WSE changes between June 7th and all subsequent dates (n = 58). c) AirSWOT WSE change differences at each PT location for all possible date combinations (n = 161). All AirSWOT WSE changes are calculated with the bias-corrected WSEs. Different colors represent the various PT locations. PT uncertainty bars are too small to visualize.

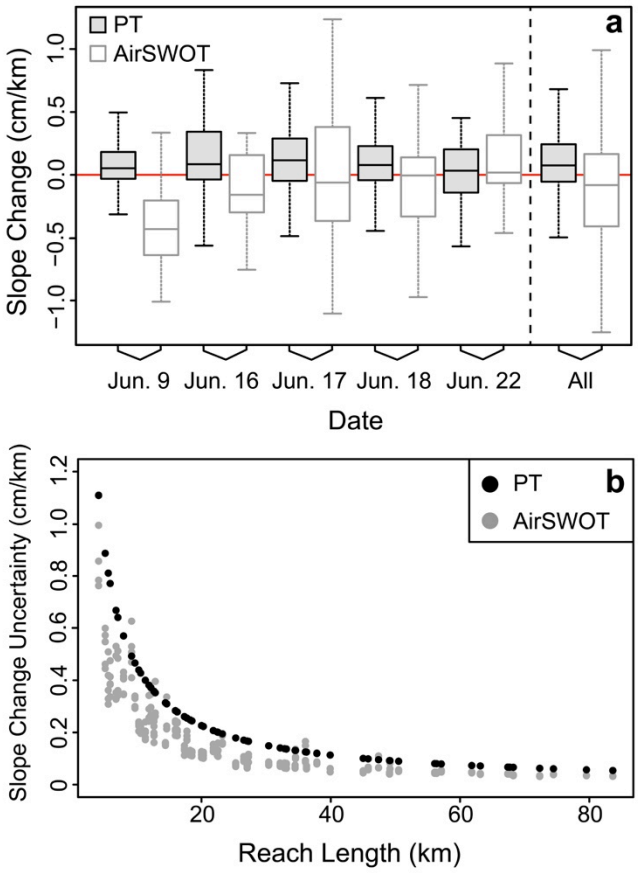

Fig. 8: a) Boxplots of observed slope changes by the pressure transducers (PT, grey) and AirSWOT (white) between June 7th and all subsequent dates (n = 297), as well as all possible date combinations (All) (n = 766). Outliers make up 15% of the data points and are not shown in the boxplots of slope change distributions. The red horizontal line designates zero slope change, while the black vertical dashed line separates the consecutive slope change distributions from the distributions for all possible date combinations. b) AirSWOT (grey) and PT (black) slope change uncertainties versus reach length.

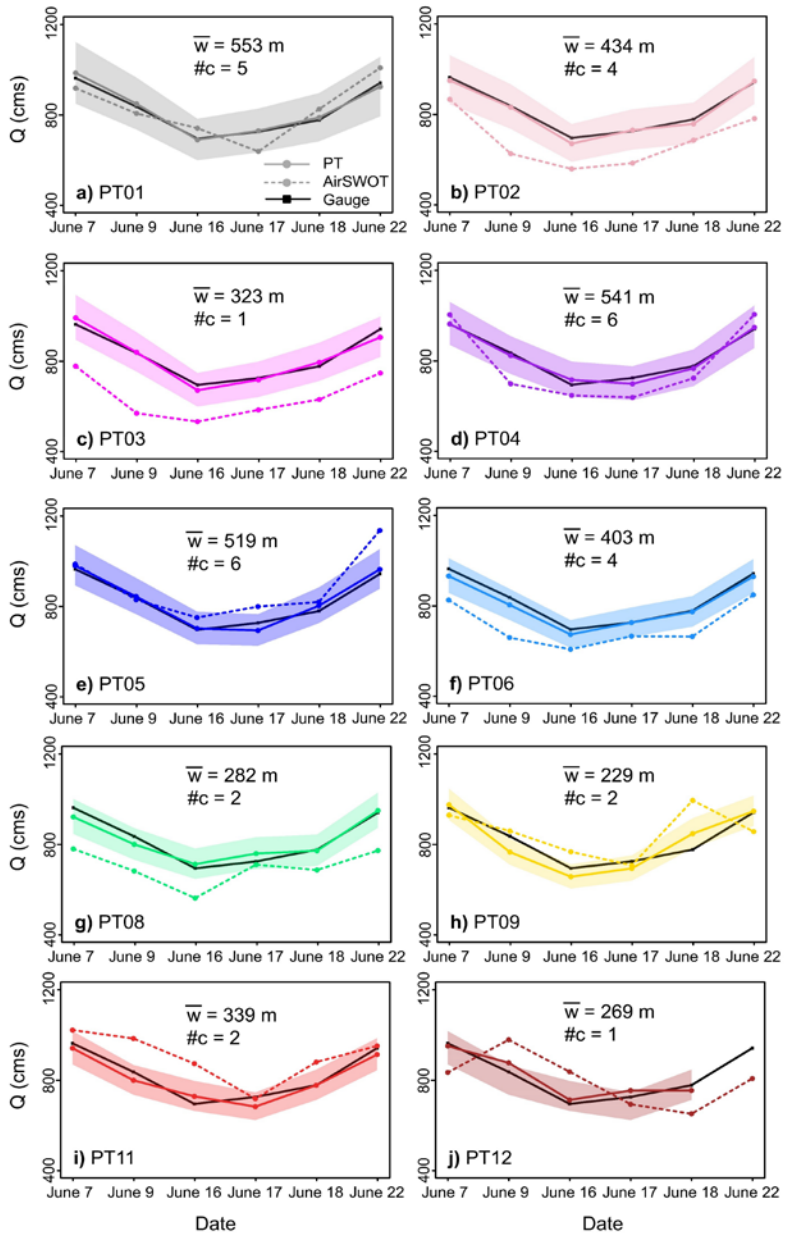

Fig. 9: Tanana River discharge estimates calculated using Manning's equation. Solid colored lines display discharge estimates using the PT WSEs and slopes, while dashed colored lines display discharge estimates using AirSWOT WSEs and slopes. Shaded colored areas indicate the PT discharge uncertainties. Nenana gauge discharge is shown as the black solid line in each panel. Average width ($\overline{w}$), and number of channels in the cross section (#c) are displayed.

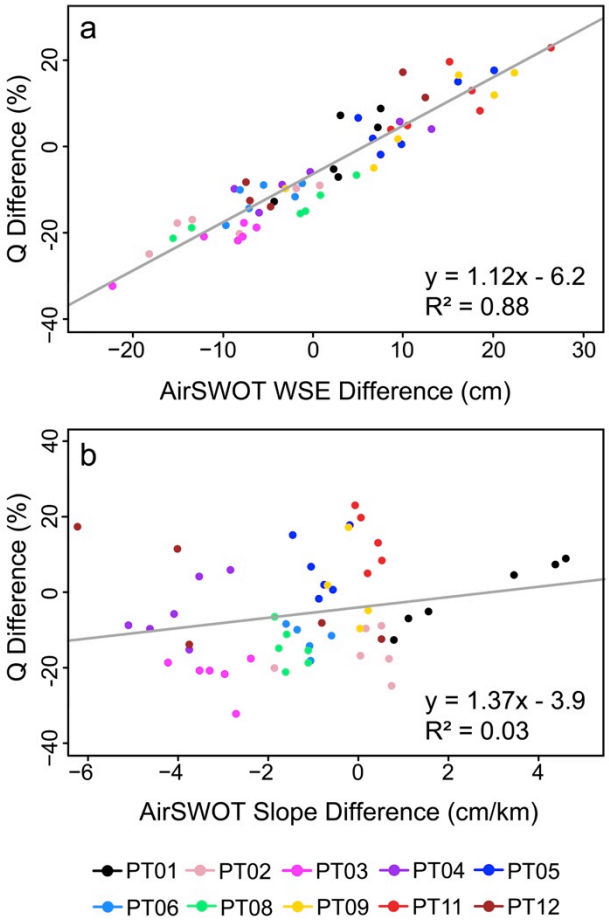

Fig. 10: The differences between AirSWOT and PT observations of WSEs (a) and slopes (b) versus differences in calculated discharge values when using AirSWOT observations versus PT observations of WSE and slope. Colored dots represent the different pressure transducer (PT) locations.